Vicinal surfaces for functional nanostructures

2009 J. Phys.: Condens. Matter 21 013002

(http://iopscience.iop.org/0953-8984/21/1/013002)

IOP PUBLISHING JOURNAL OF PHYSICS: CONDENSED MATTER

J. Phys.: Condens. Matter **21** (2009) 013002 (18pp) doi:10.1088/0953-8984/21/1/013002

TOPICAL REVIEW

Vicinal surfaces for functional nanostructures

Christoph Tegenkamp

Institut für Festkörperphysik, Gottfried Wilhelm Leibniz Universität Hannover, Appelstrasse 2, D-30167 Hannover, Germany

E-mail: tegenkamp@fkp.uni-hannover.de

Received 4 September 2008, in final form 30 September 2008
Published 1 December 2008
Online at stacks.iop.org/JPhysCM/21/013002

Abstract

Vicinal surfaces are currently the focus of research. The regular arrangements of atomic steps on a mesoscopic scale reveal the possibility to functionalize these surfaces for technical applications, e.g. nanowires, catalysts, etc. The steps of the vicinal surface are well-defined defect structures of atomic size for nucleation of low-dimensional nanostructures. The concentration and therefore the coupling *between* the nanostructures can be tuned over a wide range by simply changing the inclination angle of the substrate. However, the coupling of these nano-objects to the substrate is just as important in controlling their electronic or chemical properties and making a functionality useable.

On the basis of stepped insulating films, these aspects are fulfilled and will be considered in the first part of this review. Recent results for the epitaxial growth of wide bandgap insulating films (CaF_2, MgO, NaCl, BaSrO) on metallic and semiconducting vicinal substrates (Si(100), Ge(100), Ag(100)) will be presented. The change of the electronic structure, the adsorption behavior as well as the kinetics and energetics of color centers in the presence of steps is discussed.

The successful bridging of the gap between the atomic and mesoscopic world, i.e. the functionalization of vicinal surfaces by nanostructures, is demonstrated in the second part by metal adsorption on semiconducting surfaces. For (sub)monolayer coverage these systems have in common that the surface states do not hybridize with the support, i.e. the semiconducting surfaces are insulating. Here I will focus on the latest results of macroscopic transport measurements on Pb quantum wires grown on vicinal Si(111) showing indeed a one-dimensional transport behavior.

(Some figures in this article are in colour only in the electronic version)

Contents

1. Introduction

Vicinal surfaces have been extensively studied over the last four decades and have also attracted the focus of current research in surface science. A search for the phrase 'vicinal

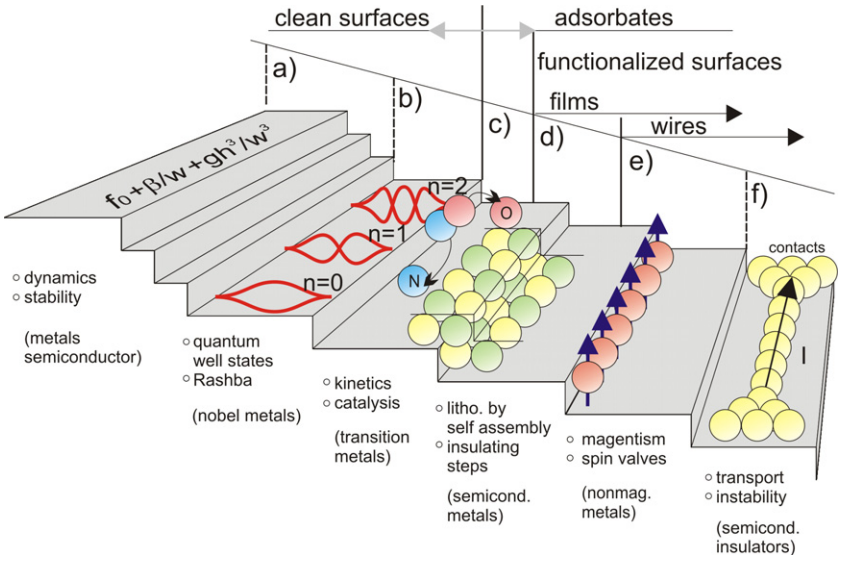

Figure 1. Schematic representing the different approaches of functionalizing vicinal surfaces. (a) Step dynamics of clean surfaces, (b) confined surface states, (c) step-enhanced chemical reactions, (d) three-dimensional epitaxy of films (this work), (e) magnetic wires and (f) atomic wires suitable for transport (this work). In brackets are named the substrates which have been used in the past to obtain the specified functionalization.

surface' in the ISI Web [1] has revealed around 2900 hits, i.e. around 2% of surface science articles published within the last ten years (1998–2007) deal with these regularly stepped surfaces. They are close to the equilibrium structure of low Miller index surfaces, and the introduction of steps is a controlled approach towards the implementation of periodically arranged defects. In particular the structure and bonding at the step sites determine crucially chemical reactions and the adsorption behavior. The periodic arrangement reduces the symmetry of the surfaces and the template becomes 1d or at least strongly anisotropic. This single-domain structure can be transferred to adsorbates, i.e. growth of atomic wires along the chain structure by self-assembly is possible. However, the residual interaction determines crucially whether the 1d structure itself leads to strong confinement effects in the electronic system. Towards transport measurements the demands are even higher, because nanostructures, at least on the mesoscopic scale, have to be grown on insulating surfaces. Furthermore, if high temperature applications are intended, only wide bandgap insulators as support can be used.

In general, to exploit the advantages of this approach for growing functionalized nanostructures, it is essential to understand the equilibrium structure of the *clean vicinal surface* itself. Many efforts have been spent on this issue in the past. Strongly stimulated by the progress made by directly imaging methods, e.g. STM [2], LEEM [3] and SEM [4, 5], but also diffraction experiments [6, 7], different theoretical models were proposed for the description of the equilibrium structures both on the atomic scale (lattice gas and solid-on-solid) [8] and as continuum models [9, 10]. Based on the free energy expression of Gruber and Mullins [11], step bunching on Si surfaces has been understood quantitatively (figure 1(a)). By taking into account strong relaxation effects on semiconducting surfaces, these concepts can be applied successfully both to metallic and semiconducting surfaces [12]. Based on these models even the stability of the steps of the vicinal surfaces and their dynamics can be predicted to some extent. For more details the interested reader is referred to the review article by Jeong and Williams [13].

The impact of steps on the electronic structure is nicely demonstrated by 1d surface states. Using (111) surfaces of noble metals like Ag, Cu and Au the Shockley-type surface and image potential states, which are trapped between the vacuum barrier and the crystal gap stemming from the projection of the s and p bands [14–17], are scattered effectively by the steps. Their regular arrangement on vicinal substrates has been used as a superlattice giving rise to 1d or even 0d confinement effects, even providing insight into the involved wavefunctions [18] (see figure 1(b)). The quantization conditions of the quasi-free electrons can be tuned in position simply by changing the inclination angle, the orientation or the material itself. Besides these quantum well states originating from strong coupling, even reconstructions, e.g. the (slightly modified) herringbone reconstruction on Au(778) along the terraces, cause multiple gaps in the electronic states (weak coupling limit), giving rise to quantum dot state effects on clean surfaces [19, 20]. By choosing materials having a high spin–orbit coupling, e.g. Au(111), Rashba-type splitting has been observed, which is interesting in the context of magnetic properties on (stepped) surfaces (see below). The influence of steps towards modifications of image potential states has been recently investigated using angle-resolved two-photon photoelectron spectroscopy [21]. An excellent overview of the topic of quantum well states on vicinal noble metal surfaces can be found in [22].

Towards a functionalization of vicinal surfaces there have been recently reported promising attempts at growing perfect metallic chains along the step structure of metallic surfaces. Compared to, for example, semiconductor surfaces, relaxation effects on metallic surfaces are comparably small [13]

and therefore the decoration of these steps by adatoms is understood for many systems quantitatively in terms of adsorption theory. Transition metals with their characteristic d-band structure at step edges turn out to be ideal templates. For instance, for vicinal Pt(111) perfect growth of atomic chains of Ag, Co, Cu, Fe and Mo atoms has been demonstrated [23] (figure 1(e)). A genuine approach towards a technologically relevant functionality, e.g. spin valves, has been demonstrated using atoms with high spin momentum. Progress has been obtained in this field of low-dimensional magnetic structures recently both experimentally and theoretically [24–29]. For atomic chains showing an (anti-)ferromagnetic order the anisotropy mediated by the shape of the structure, the surface or by the step itself is being decisive. For instance, the orbital and the spin moment per Co atom on a vicinal Cu(111) surface is increased by 25% due to the break of the translational symmetry by atomic steps [30]. However, although the growth of atomic chains by self-assembly can be controlled perfectly, these systems are not suitable for any electric transport measurements. For this issue insulating substrates, i.e. semiconductors or wide bandgap insulators, are necessary. Details on the preparation and functionalization of templates, which do not hybridize with the electronic states of nanostructures at least around the Fermi energy, are within the scope of this review in section 2 and section 3, respectively.

The lower coordination of atoms at step sites change the electronic and *chemical properties* and determine to a large extent the growth of nanostructures, e.g. of atomic wires, along the step edges and even of multilayers. Langmuir and Taylor were the first who considered the influence of steps on chemical reactions [31, 32] (figure 1(c)). In the context of chemical reactions the advantage of using vicinal surfaces is primarily not the step regularity but rather the possibility to change the step densities gradually as a function of the inclination angle. In the simplest model, the spill-out of (s-type) electrons at step edges reduces the work function of metallic surfaces, as considered first by Smoluchowski [33]. However, to explain the catalytical activity of transition metals, the contributions of the d-electrons have to be considered. For instance, the enhanced reactivity found for the CO adsorption on vicinal Pt(111) surfaces at step sites is explained by a coordination-induced change in the d-hole density [34–36]. Steps may even lower the dissociation barrier as was seen for the NO dissociation step edges on Ru(0001) by STM [37]. In the case of molecular oxygen, clean Pt steps enhance the dissociation by stabilizing the precursor state of molecular oxygen rather than by lowering the barrier energy, while pre-decoration of these steps with Ag lowers the reactivity by one order of magnitude [23, 38]. These examples show that the interplay of the electronic states of the surface, the steps and the adsorbates is important but rather complex.

This complexity can be lifted to some extent using insulating films instead, e.g. binary wide bandgap insulators, which are chemically inert, experimentally easy to prepare and therefore an ideal support to built up modularly the nanoreactor on the surface. That at least defect-free insulating films do not almost interact with adatoms or molecules has been demonstrated by our own work in the past [39] and more recently demonstrated in an impressive STM/STS study for single pentacene molecules adsorbed on NaCl(100) films grown on Cu(100) [40]. It was shown further that a single surface anion vacancy as a model defect preferentially binds these adatoms and molecules. The changes in the electronic structure of the adsorbate, however, are comparably small and for closed films with thicknesses of only a few atomic layers the substrate does not interact at all. Although the influences are small, they can determine to a large extent the chemical activity. For instance, in the cyclomerization of ethylene at Pd clusters on MgO films the clusters themselves are only catalytically active, if an anion vacancy is underneath [41, 42]. Whether steps are at all important for such processes has not been investigated systematically so far, presumably because of the lack of appropriate stepped insulating films. Beyond this, well-defined stepped insulating films might be used to grow low-dimensional metallic chains instead of clusters. This concept can be combined with anion vacancies, which can selectively enhance binding strengths and reactivities at step sites. In section 2, I will highlight recent progress made for growing regularly stepped insulating films and show that the reactivity can indeed be triggered by the step density.

An ultimate scenario of a functionalized nanostructure is the growth of metallic wires by self-assembly along the step direction that are suitable for unidirectional electric transport. As theory predicts new physical phenomena in 1d structures, several attempts were begun to investigate their properties using atomic chain structures either in strongly anisotropic (organic) solids [43] or those grown on vicinal surfaces. With respect to transport properties a Luttinger liquid behavior is expected rather than a Fermi liquid behavior [44]. In addition, at least free-standing, i.e. weakly interacting, one-dimensional structures often undergo a metal–insulator phase transition as a function of temperature. Using magnetic adsorbates, even long range ferro- and antiferromagnetic coupling is suppressed at finite temperatures [46]. To overcome this ambivalence, the growth of atomic wires on vicinal surfaces can be a way out, since an appropriate interaction may suppress these instabilities but not the 1d properties.

This approach already comprises two extreme requirements, namely the growth of chains with a thickness and width of a few atoms, to reveal a robust quantization condition for the electrons, and the growth of long wires, e.g. in the range of microns, to allow a reliable positioning of ohmic contacts, e.g. by lithography [47–49]. Although many technical problems will show up, semiconductor substrates are advantageous. First, silicon samples are insulating below 200 K when using low-doped silicon samples, i.e. the contribution of the substrate is typically three orders of magnitude lower relative to the contributions of the metallic adlayers and can be well discriminated. Second, they allow us to prepare straight step structures under UHV conditions due to the high kink formation energies [50, 51]. Finally, by using different orientations or inclination angles the interaction can be tuned gradually. This parameter is, in particular, important when instabilities are the focus of research. However, the adsorption of metals onto semiconducting surfaces is more complex compared to metallic surfaces, as it leads

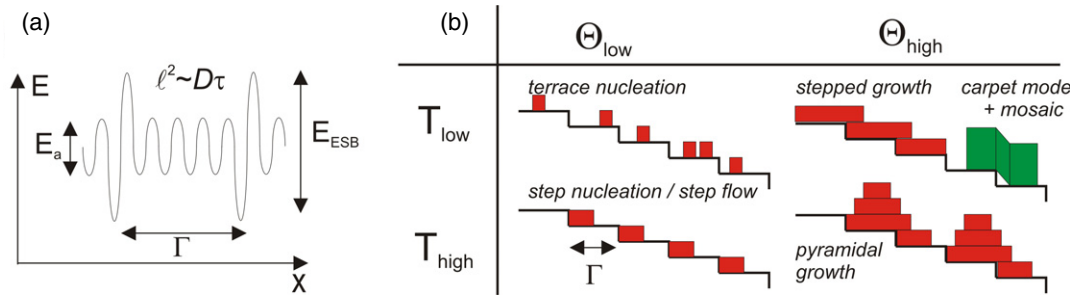

Figure 2. (a) Simplified energy landscape of a vicinal surface determined by the terrace diffusion energy E_a and the Ehrlich–Schwoebel barrier E_{ESB}. (b) Rough classification of different growth modes of insulating materials found on vicinal substrates for two different temperature (T) and coverage (Θ) regimes. The exact definition of high and low temperature and coverage, respectively, depends on the system and the vicinality. For further details see the text.

usually to strong relaxation effects with large unit cells. Furthermore, the electronic bands are strongly hybridized with the substrate, i.e. the total transport in these systems is, in general, determined by contributions from surface states, space charge layers and even bulk states. In limits the latter two contributions can be tuned by the type and concentration of the dopants [52, 53]. More details about metal/semiconductor interfaces are presented in section 3. Nonetheless, as will be demonstrated for the adsorption of Pb on vicinal Si(111) substrates, they allow us to bridge the gap between the atomistic and mesoscopic world and fulfill the conditions to study the transport within quantum wires, as sketched in figure 1(f).

This review is organized as follows: in section 2 recent results of the growth of insulating films on vicinal substrates will be presented. Both the monolayer and the multilayer regime are considered. In particular the important parameters towards a perfect growth of stepped epitaxial films are presented and changes of the electronic structure, the reactivity and kinetics of color centers on vicinal wide bandgap insulators are discussed. A functionality of metallic quantum wires is finally demonstrated in section 3 by macroscopic transport measurements for Pb wires on Si(557). Whereas above 78 K anisotropic transport is found along the wires and in the perpendicular direction, the system shows only conductivity along the wires below 78 K. Both transport regimes can be explained by the electronic band structure. Furthermore, the switching in conductance is due to a temperature-driven refaceting transition as revealed by the latest LEED measurements.

2. Insulating films on vicinal substrates

The growth of multilayer films on vicinal substrates has only recently attracted interest. As mentioned in the context of functionalization of vicinal surfaces, insulators with tunable step densities are attractive templates. In the following three sections I will briefly summarize the progress made in growing vicinal insulating films. In particular the influence of the lateral *and* vertical lattice parameters towards the epitaxial growth on vicinal supports is considered. The functionality of these insulating vicinal structures is demonstrated by studying the kinetics of color centers at step sites as well as enhanced step energies seen by thermal desorption spectroscopy.

2.1. Growth modes of insulators on vicinal substrates

In general, the diffusion of adatoms on terraces is determined by the terrace diffusion energy E_a (cf figure 2(a)). The corrugation of this potential is higher for semiconducting surfaces than for metallic surfaces, because of strong relaxation effects. Furthermore, Ehrlich–Schwoebel barriers E_{ESB}, i.e. enhanced diffusion barriers for adatoms or molecules at step sites (see figure 2(a)) [54, 55], have to be taken into account. A step flow regime is obtained only for higher temperatures resulting in step decoration as sketched in figure 2(b). Besides, if the average diffusion length $\ell \sim \sqrt{D\tau}$ is of the order of the average terrace length, stable nuclei can be formed on the terraces. However, exact growth parameters depend crucially on the system, the step density, the temperature and the deposition rate. One textbook example is the adsorption of CaF_2 on stepped Si(111) in the submonolayer regime, revealing both growth modes as sketched on the left of figure 2(b) and shown by STM images in figure 3. At $T = 830$ K step decoration of 0.1 TL (triple layer) CaF_2 is found whereas at lower temperatures this mode is suppressed and homogeneous nucleation on terraces sets in. From the investigation of the dependence of this critical temperature as a function of the terrace width Γ a diffusion barrier of $E_a = 1.8$ eV is proposed [56]. Recent experiments have shown [57] that the step flow mode can be used to grow almost perfect, i.e. nanostripes microns in length of CaF_2 along straightened Si(111) steps [50, 51]. With respect to metal adsorption on metallic substrates the adsorption of CaF_2 on stepped Si(111) substrates is more challenging, because the (7×7) reconstruction of Si(111) surfaces must be annihilated upon adsorption and a CaF interface layer is formed in order to have a perfectly sharp and lattice matched interface, as analyzed in detail by TEM, XPS and XPD [58–60].

To grow *closed* epitaxial films the lattice mismatch between the adsorbate and the substrate is essential. From an energetic point of view, insulators with low surface energies, grow layer by layer on metallic or semiconducting substrates. Such insulators have in common their ionic and/or strongly covalent bonding character, i.e. pseudomorphic growth does

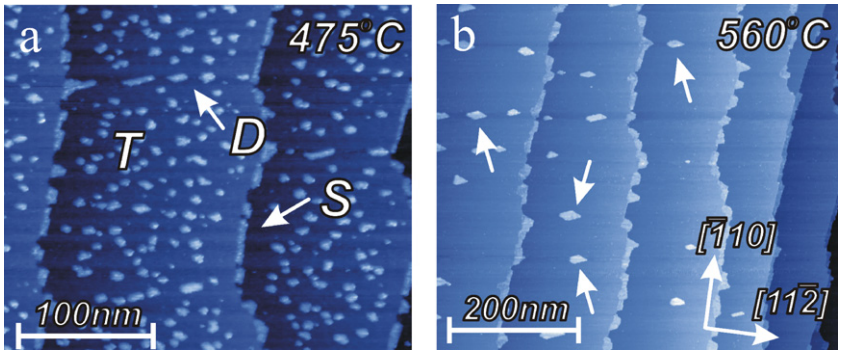

Figure 3. STM images of 0.1 TL CaF_2 deposited at 650 and 830 K on vicinal Si(111). (a) Homogeneous nucleation on terraces (*T*) is dominant. Further nucleation occurs at heterogeneous sites as steps (S) and anti-phase domain boundaries (D). (b) At 830 K the homogeneous nucleation on terraces is suppressed. The islands are nucleated only at steps and domain boundaries. The arrows show the formation of islands with partial *A* and partial *B* orientation nucleated at anti-phase domain boundaries. Reprinted with permission from [56]. Copyright 2002 Springer.

not take place. Therefore, depending on the substrate, the mismatch should be as low as possible for epitaxial growth. For the growth on metallic substrates, sufficiently large grains can be grown if the (lateral) mismatch is of the order 3%. One example, which is discussed in the following, is the growth of MgO on vicinal Ag(100) surfaces. In contrast, for the growth on semiconducting substrates, the mismatch should not exceed 1% because of stronger interface bonds, as will be shown for the growth of NaCl on vicinal Ge(100) surfaces with different inclination angles. As a proof of concept, finally the perfect growth of lattice-matched BaSrO mixed oxide layers on vicinal Si(100) substrates is presented.

However, only if a *vertical lattice accommodation* is also achieved does layer-by-layer growth take place on vicinal substrates. This is in a simple manner the case for MgO/Ag(1, 1, 19), as it has the same crystal structure. The situation is more complex using semiconducting substrates, e.g. Si and Ge. For insulating films with rock-salt structures, e.g. NaCl, the energetically stable (100) termination of these surfaces forces one to use (100) oriented substrates, but with steps of double atomic height. Though for CaF_2/Si(111) the step structure matches perfectly with the step height of the CaF_2(111) layers, the films can grow in two orientations due to the fluorite crystal structure. Depending on the inclination direction of the sample ($[\bar{1}\bar{1}2]$ or $[11\bar{2}]$) only one configuration can overgrow the steps for stoichiometrical reasons, e.g. if the Si(111) substrate is tilted towards the $[11\bar{2}]$ direction only the so-called B-type configuration forms closed films and pitch holes at step edges, which causes high leakage currents in device structures, e.g. resonant tunneling diodes, to be suppressed.

In the following, three examples of multilayer growth on vicinal substrates will be emphasized. All experiments have been performed under UHV conditions. The morphology is analyzed by means of SPA-LEED, as the problem of tunneling with atomic resolution on thick insulating layers is circumvented and the average of the morphological quantities, which are important for any functionalization on a mesoscopic scale, is obtained. To avoid difficulties during growth by using only cation or anion decorated surfaces, only non-polar (100) orientated surfaces have been investigated. For further details about the preparation of the substrates, etc, the reader is referred to [61–63].

MgO/Ag(100)-[011] 5.8°. The clean Ag(1, 1, 19) surface consists of (0 0 1) terraces with close-packed steps in the $[\bar{1}10]$ direction. The nominal average terrace length is 9.5 atoms or 28.3 Å for steps of monatomic height [7]. The average terrace length is small enough to expect a higher step density for the MgO films grown on this substrate compared to a Ag(100) surface, but at the same time it is large enough so that the MgO films can relax on the single terraces and an accumulation of steps due to step–step interaction is not expected to occur. This system is therefore ideal to expect a layer-by-layer growth as for MgO on nominally flat Ag(100) surfaces [64]. In particular the interplay between the $[\bar{1}10]$ step direction of the substrate should favor the formation of polar steps in the MgO film, assuming that they are formed on the atomic scale with the same orientation as the substrate steps. Any zig-zag structures of the steps composed of only non-polar step edges in [100] and [010] directions increase the length of the step edges, but would cost less energy per unit length than the formation of polar steps.

Films were produced by *in situ* oxidation (pressure 1×10^{-7} mbar) close to room temperature and the stoichiometry was controlled by x-ray photoelectron spectroscopy (XPS). No splitting of the O 1s and the Mg(KLL) peaks has been observed as would be characteristic for a metallic or non-stoichiometric component [65]. From the investigations of the bandgaps in MgO layers by electron energy loss spectroscopy (EELS) there are no indications of a spontaneous formation of point defects with concentrations above the detection limit (0.1%) during the growth process. Furthermore, from the low cross sections determined in earlier investigations of electron-induced formation of surface F-centers [66], we can rule out any electron-beam-induced influences on the growth of the MgO layers.

Figure 4 shows SPA-LEED results obtained for 5 ML MgO grown on Ag(1 1 19). Besides the (1×1) structure, all integer peaks contain a substructure, visible in 2d LEED patterns as halo structures, as is shown exemplarily for the (00)

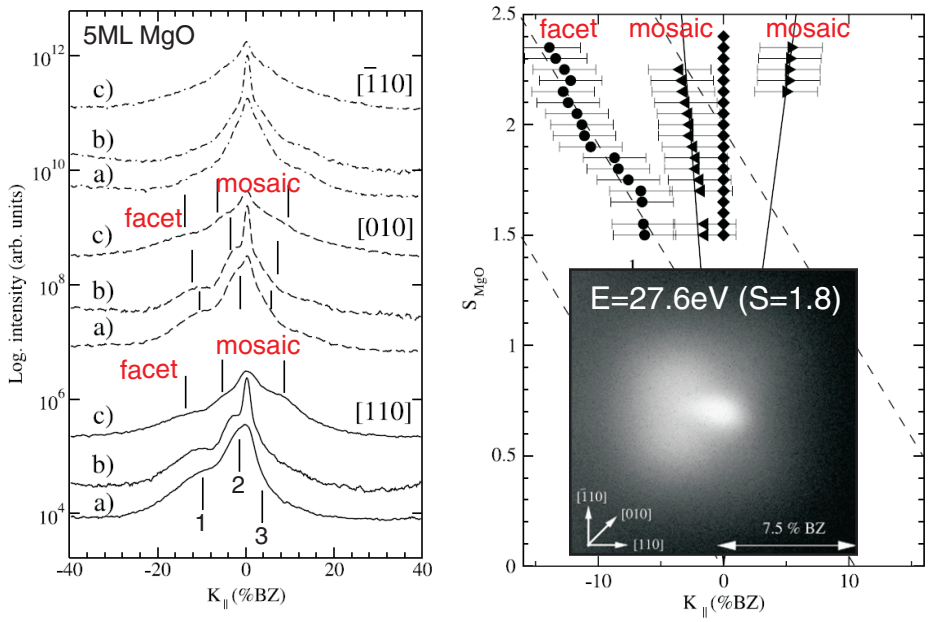

Figure 4. (Left) Spot profiles of the (00) spot of 5 ML MgO/Ag(1, 1, 19) taken along different crystallographic directions and different energies: (a) 26 eV ($S = 1.75$), (b) 34 eV ($S = 2$), (c) 43 eV ($S = 2.25$). (Right) The positional variation of the satellite peaks follows the dashed and solid lines, which correspond to (1, 1, 19) facets and mosaics, respectively. The inset is a magnification of the (00) spot, showing a characteristic halo structure.

spot in the inset of figure 4. From the line scans taken along different directions and different energies, shoulders assigned as 1, 2 and 3 become visible. Systematics of the shift of the satellites can more easily be analyzed when plotting the locations of these peaks versus their scattering phase. This is done in figure 4 for the line scans in the [110] direction. As is seen from this figure, the variation of satellite 1 as a function of $k_{\perp}$ follows closely one of the dashed lines, which mark the facet rods of the Ag(1, 1, 19) surface. By comparison with XPS, UPS and EELS data of MgO films on the flat Ag(100) surface, the corresponding spectra for the 5 ML thick MgO film are characteristic for a completely closed film and provide no evidence for uncovered parts. This leads to the conclusion that the film consist of facets with a similar step density as the silver surface. As seen from the inset in figure 4, the facet orientation has some preference for the [1 0 0] directions, but there is clearly intensity also in the [1 1 0] direction, meaning that the MgO step edges also have polar orientations. In contrast, the growth of thinner layers results in not completely closed films. Instead the formation of pyramidal structures with non-polar step edges has been observed [61].

Satellites 2 and 3 of figure 4 point to mosaics as their positions of a function of $k_{\perp}$ fall on lines through the origin. The formation of mosaics is the result of the finite lattice mismatch of 3% and has been found on flat Ag(100) substrates as well [64]. However, the observed angles found on vicinal substrates are significantly smaller ($\theta \approx 0.5°$ (satellite 2) and $\theta \approx 0.9°$ (satellite 3)). This difference in mosaic angles is mainly due to the step structure of the underlying substrate. The easy glide planes of MgO for formation of dislocations are the (1 1 0) planes. Since silver is a soft material compared with MgO, these dislocations can be more effectively pressed into the substrate at step edges than on a flat Ag surface. This results in a decreased bending of the film to compensate for the misfit. Atoms of the Ag(1, 1, 19) surface near steps have more flexibility to relax towards the preferred lattice position in order to minimize the surface energy.

NaCl/Ge(100)-[011] 5.4°. For an epitaxial growth of NaCl, Ge(100) substrates are perfectly matched templates. The mismatch is only 0.3% and thus mosaic formation is not expected. For growth experiments of stepped films, vicinal Ge(100) surfaces have been used. Any NaCl-induced refaceting of the surface, like has been found for NaCl/Cu(311) and Cu(532) [67, 68], does not occur on these semiconducting surfaces. For details about the cleaning procedures of the samples as well as the deposition of NaCl see [62]. To illustrate the influence of different step densities, films were grown on flat Ge(100) substrates and on Ge samples with a miscut of 2.7° and 5.4° along the [011] direction. Exemplarily, for the latter a LEED pattern is shown in figure 5(a). Unfortunately, Ge samples even with a miscut angle of 5.4° still contain a large fraction of monatomic steps [6] that are only half as high as the minimum step height in NaCl. From previous investigations it is known that these monatomic steps are simply overgrown in an elastically bent mode (so-called carpet mode) [69, 70] so that NaCl steps are not generated.

The clean vicinal Ge(100) samples themselves have been studied intensively by means of LEED [6, 7]. From the terrace width distribution we have estimated the step energies, which are, compared to vicinal Si(100) substrates, an order of magnitude lower, i.e. the critical angle of Ge(100) to form a single domain structure with D_B-type steps is around 9° and, as a result, the (100) terraces are too short to allow an epitaxial growth of NaCl. However, the fraction of the

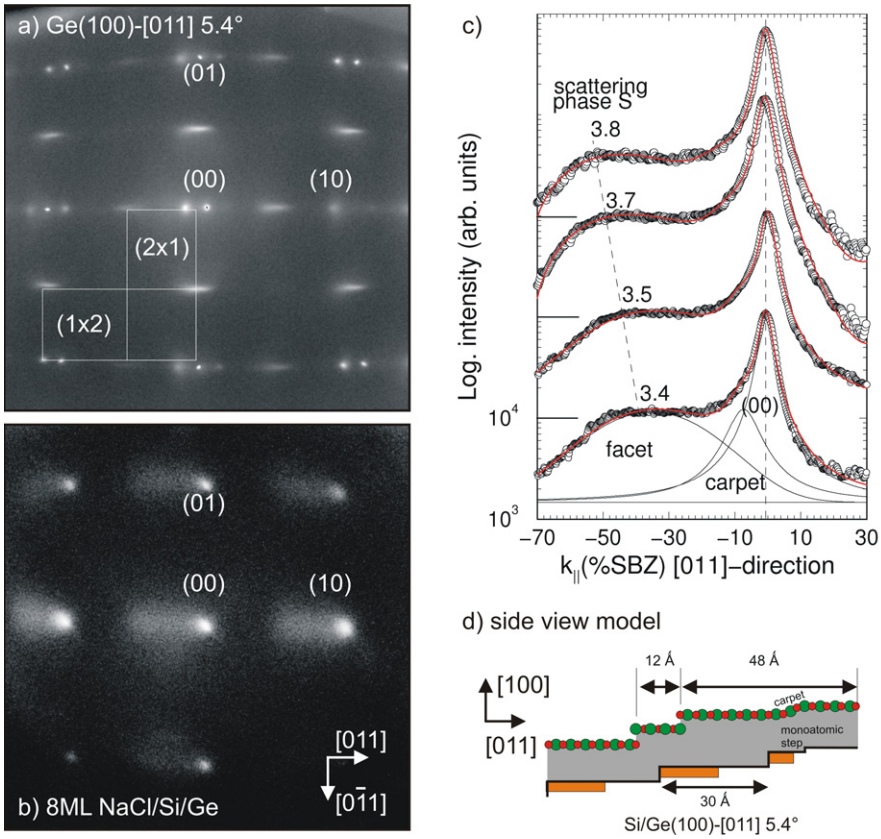

Figure 5. (a) 2d LEED pattern of the clean vicinal Ge(100) surface ($E = 230$ eV). (b) Halo structure after adsorption of 8 ML NaCl at 200 K. Prior to NaCl adsorption, 0.5 ML Si was adsorbed to reveal a single domain structure with steps of double atomic height. (c) Profiles taken across the step direction for different scattering phases. (d) Shows the structural model deduced from a detailed profile analysis [62]. Besides the (611) facet with polar steps the carpet mode expected for a monatomic Ge step is shown as well.

monatomic steps on the Ge surfaces with moderate inclination angles can be reduced by evaporation of Si onto the vicinal Ge surface prior to NaCl film growth. The alternating arrangement of the (1 × 2) domains, when steps of single atomic height are present, causes an anisotropic diffusion for Si adatoms. As explained in more detail in [71], the evaporation of approximately 0.5 ML Si at 470 K results in the population of the next but one terrace, i.e. in the formation of a single domain heterostructure with steps of double atomic height in between.

This type of sample has been used successfully for growing stepped NaCl films at substrate temperatures around 200 K. The LEED pattern (cf figure 5(b)) obtained after the deposition of 8 ML shows a (1 × 1) structure with an extended intensity distribution along the step direction of the underlying substrate, to some extent similar to the halo structure seen for MgO on Ag(1, 1, 19). As can be seen for the profiles taken along the [011] direction around the (00) spot in figure 5(c) the halo intensity shifts linearly by increasing the scattering phase S (given with respect to the NaCl step height (2.82 Å)). The tilt angle with respect to the (00) rod is 13°. Taking into account that, due to residual monatomic steps of the Si-precovered surface the elastically bent carpet mode is also present, the main facet structure can be described well by a (611) facet, which is different from the facet structure of the Ge surface itself.

Interestingly, if the bulk NaCl structure is maintained at the surface, this facet orientation corresponds to alternating rows of Na^+ and Cl^- ions at distances of 12.2 Å. From the FWHM of this peak around 30% SBZ at an out-of-phase condition it can be deduced that the mini-facets consist mainly of one pair of such ionic steps. This means that on this scale NaCl double steps are formed, whereas single ionic step edges seem to be avoided. Obviously, the electrostatic interaction favors this new facet structure. The result is consistent with the estimate of the average size of the unit mesh in the [011] direction, which is the sum of the average terrace width plus one mini-facet. The average terrace width obtained from the FWHM of the (00) beam at an out-of-phase condition is 45 ± 5 Å, from which an average length of the unit mesh close to 60 Å is deduced. This is twice the distance between double steps on the Ge substrate surface. Thus we obtain a model for the NaCl film that overgrows, on average, two double steps of the substrate when a mini-facet with polar steps is formed. A schematic of the 8 ML thick NaCl film in this growth mode is shown in figure 5(d).

It should been mentioned that only on the Si-preadsorbed vicinal Ge samples does the NaCl facet structure appear. For instance, using vicinal Ge(100) samples with only 2.7° miscut, i.e. the surface exhibits both S_A-and S_B-type steps, only the elastically bent carpet mode has been found. The growth of NaCl on these vicinal Ge(100) surfaces at room temperatures

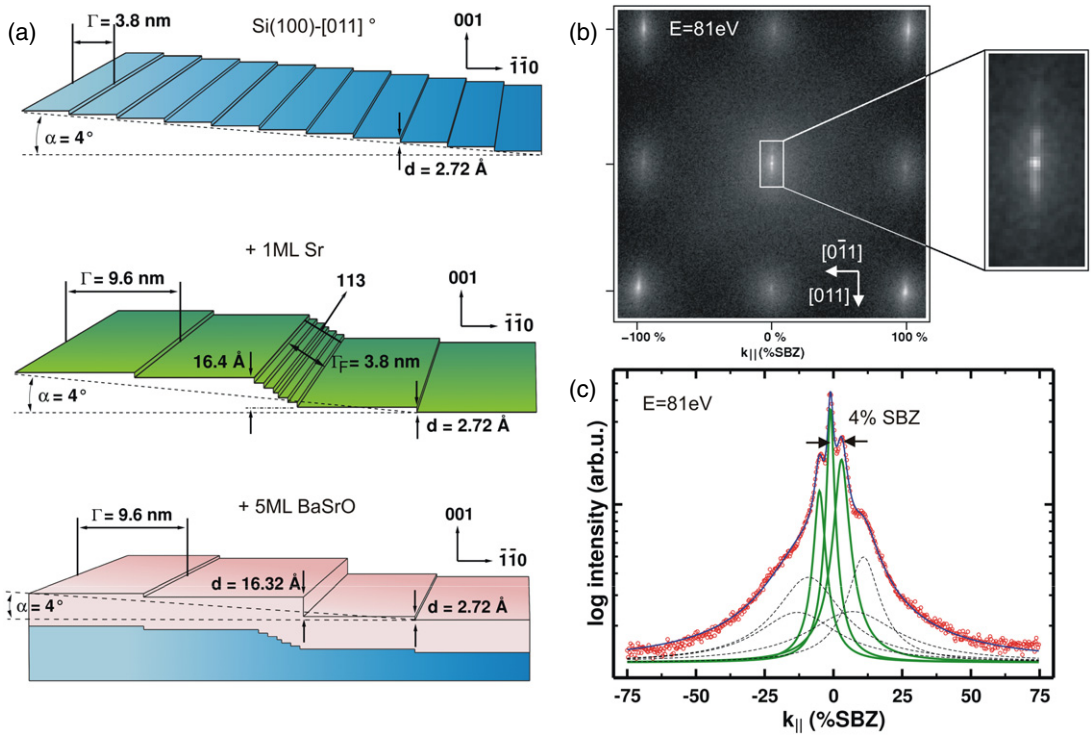

Figure 6. (a) Schematic of the change in the step structure of the vicinal Si(100) surface (top) upon adsorption of 1 ML Sr (middle) and the $Ba_{0.7}Sr_{0.3}O$ film (bottom). (b) 2d LEED pattern of 10 ML of $Ba_{0.7}Sr_{0.3}O$. (c) Profile taken along the [011] direction. From the spot splitting the model shown at the bottom of (a) is deduced. For further details see the text.

results in pyramidal growth as is sketched in figure 2(b). The LEED of this phase pattern reveal around all integer spots a characteristic broadening of the peaks mainly in the [0$\bar{1}$0] and [00$\bar{1}$] direction, similar to the growth of MgO/Ag(1, 1, 19). From plotting the FWHM of the (00) diffraction peak versus the scattering phase, we examined an average terrace length of 60 Å (along the [011] direction), which is larger than the terrace length of the underlying for a still epitaxial, but rough surface. Since the preferential step direction in this growth mode is now the non-polar step direction, we conclude that the Si/Ge steps are overgrown by pyramids of NaCl [62].

$Ba_{0.7}Sr_{0.3}O$/Si(100)-[011] 4°. Compared to Ge(100) surfaces, vicinal Si(100) surfaces seem to be promising candidates, since their high step energies and strain effects of the terraces result in a much lower critical angle of 4°. The terrace length for this surface is around 40 Å (10 nearest lattice sites).

Unfortunately, (lateral) lattice-matched insulating materials for these perfect templates are not easily available. Therefore, mixed $Ba_{0.7}Sr_{0.3}O$ layers were generated by evaporating the metals in oxygen ambient pressure (1×10^{-7} mbar) at room temperature. The particular mixing ratio is justified by the lattice constants for BaO of $a = 5.54$ Å and SrO of $a = 5.16$ Å in order to get an oxide with the average lattice constant of silicon $a = 5.43$ Å. However, good crystallinity with perfect lattice matching is only obtained when starting with preadsorbed metallic layers at a concentration close to one monolayer (ML), e.g. starting from the Sr(5×1) or Sr(2×1) structure [72]. These layers are needed in addition for passivation, i.e. to avoid the formation of SiO_2 species at the interface, but cause, in contrast, some refaceting of the surface. The SPA-LEED analysis has shown that approximately 10% of the surfaces are covered thereafter with [113] facets. To conserve the average inclination, the residual surface area consists of steps of double atomic height separated by 96 Å, i.e. 24 atomic units as seen by the spot splitting of approximately 4% SBZ (cf figure 6(a)).

The XPS analysis shows that a sharp interface is formed during the initial growth of the mixed oxide on the stepped Si(100). The chemical species present at the interface are up to 0.5 ML of mono-oxidized Si and 1 ML of a mixed SrOSi species. No silicide and silicate species, or SiO_2 formation at the interface after oxidation, is found. Starting already at 1 ML of $Ba_{0.7}Sr_{0.3}O$, the bandgap was found to be 4.3 eV, independent of layer thickness with no interface states within the bandgap, which underlines the perfectness of the interface.

This system offers the possibility to grow even very thick insulating layers with low roughness on these stepped silicon substrates. Figure 6 shows a LEED pattern of a 10 ML $Ba_{0.7}Sr_{0.3}O$ film. In contrast to the LEED pattern obtained from the stepped MgO and NaCl films, the halo structure is completely missing. Instead a clear spot splitting of 4 % SBZ is found. The Sr-induced [113] facets are simply overgrown by four- and sixfold steps. The sharp spot splitting as well as the large steps is nicely demonstrated by the line scan through the (00) spot shown in figure 6(c). The roughness of these surfaces has be determined by a G(S) analysis, including also variations within the layer spacings [73, 63]. For the 10 ML thick $Ba_{0.7}Sr_{0.3}O$ a rms roughness of $\Delta = 1.1$ ML

Table 1. Growth modes of insulating films on different substrates depending strongly on the lateral (lat.) and vertical mismatch (vert. misf.). $\Theta_{crit.}$ denotes the critical layer thickness for a closed film.

System	lat. (%)	vert. misf. (%)	$\Theta_{crit.}$ (ML)	Growth mode
MgO/Ag(100)-vic.	3	0	5	RT: $\Gamma_{film} = \Gamma_{sub}$ non-polar steps + *mosaics*
NaCl/Ge(100)-vic.	0.3	50	4	200 K: *carpets* $\Gamma_{film} = \Gamma_{sub}$
NaCl/Ge(100)-vic. + Si	0.3	0	8	200 K: (611) facets polar steps 300 K: pyramids non-polar steps
BaSrO/Si(100)-vic. passivated by Sr	0	0	4	300 K: $\Gamma_{film} = \Gamma_{sub}$ polar steps

is found. These numbers show that high quality crystalline mixed oxide films can be grown, which are completely closed already at thicknesses below 4 ML. The fact that the halo features have not been found in LEED shows that the step quality of the insulating film can be controlled to a large extent by the roughness of the supporting substrate although the [011] direction is the polar direction for the BaSrO system.

For all three systems epitaxial growth has been found. In particular, for MgO and the mixed BaSrO films, the terrace length can be determined by terrace width of the underlying substrates, i.e. the step and terrace energies of the insulating films are significantly lower compared to those of the substrates. Whether higher inclination angles of the substrates themselves would trigger a step growth with different terrace lengths has not been tested so far. Within this context the growth of NaCl on Si-precovered vicinal Ge(100) substrates is quite interesting: the step structure of the (611) facet is completely decoupled from the substrate, because of the formation of non-equally separated *polar* steps. If only this electrostatic contribution is important, the work necessary per unit length is equivalent to charging a capacitor consisting of two straight wires [62]. Compared to the competing carpet growth mode found for NaCl on stepped Ge(100) surfaces, the formation is approximately 1 eV $Å^{-1}$, significantly lower than in the case of a carpet (32 eV $Å^{-1}$). This energy will be further reduced if the steps are rough so that short sections of alternating dipoles exist. Of course this model cannot explain the average separation of the charges forming the dipoles, since the exact mechanisms counteracting a closer separation are not known so far. As it turns out, the concurrence of the straight step direction of the substrates with the polar step direction of the insulating films prevents the generation of perfect insulating steps, at least on a larger scale. Instead, they tend to relax into zig-zag structures, which may shorten adjacent terraces. Using insulators, whose non-polar step direction coincides with the nearest-neighbor step structure of the substrates, is a reasonable strategy but will destroy the lateral and vertical lattice accommodation. A way out of this dilemma may be the use of insulators with stronger covalent bonds in future, which stabilize the step structure. Closing this section, the growth modes obtained for closed insulating films on vicinal substrates are summarized in table 1.

2.2. Spectroscopic and chemical properties of insulator steps

As judged from the growth modes, the step energies are small and, therefore, the spectroscopic signatures are expected to be small. Because of the variety of growth modes found for NaCl/Ge(100)-vic., these systems have been characterized by means of electron energy loss spectroscopy (EELS) to see directly the influence of steps on electronic excitations. Compared to NaCl films grown on nominally flat Ge(100) substrates, the exciton excitation at a loss energy of 7.8 eV shows a broadening that is monotonically related to the step density. The FWHM increases by 20% compared to the exciton loss of a defect-free NaCl(100) surface, while the relative integral intensity of the exciton peak decreases. Both quantities are shown in figure 7 as a function of the step density. The reduction of the lifetime of the exciton with increasing step density can be understood in terms of disorder, which reduces the transfer integrals between adjacent terrace sites. A similar behavior has been found recently for Frenkel excitons in disordered polymers [76]. The change of the transfer matrix is accompanied also by an energetic shift, which is, however, below the resolution limit of our EELS instrument.

A more noticeable step response has been obtained for stepped MgO films grown on Ag(1, 1, 19) by studying losses of color centers and probing their binding strengths using thermal desorption spectroscopy (TDS). The valence state of MgO is almost 2, i.e. a singly coordinated surface anion vacancy can be either neutral (F_S), singly ionized (F_S^+) or doubly ionized (F_S^{2+}). The same argument holds for aggregates of color centers, namely M- (2 F-centers) and R-centers (3 F-centers). Agglomeration of these atomic-sized cavities for electrons leads, of course, to significant shifts of the occupied and unoccupied states. Consequently, in the case of stepped surfaces the different coordination of F-centers causes energetic shifts, which will be used in the following to characterize these steps.

Such color centers on stepped MgO films were generated by electron bombardment at room temperature using a thoriated tungsten filament, placed in front of the sample. EELS was used to detect the characteristic losses and the annihilation of color centers. Since we correlate the coordination of color centers by detecting electronic transitions

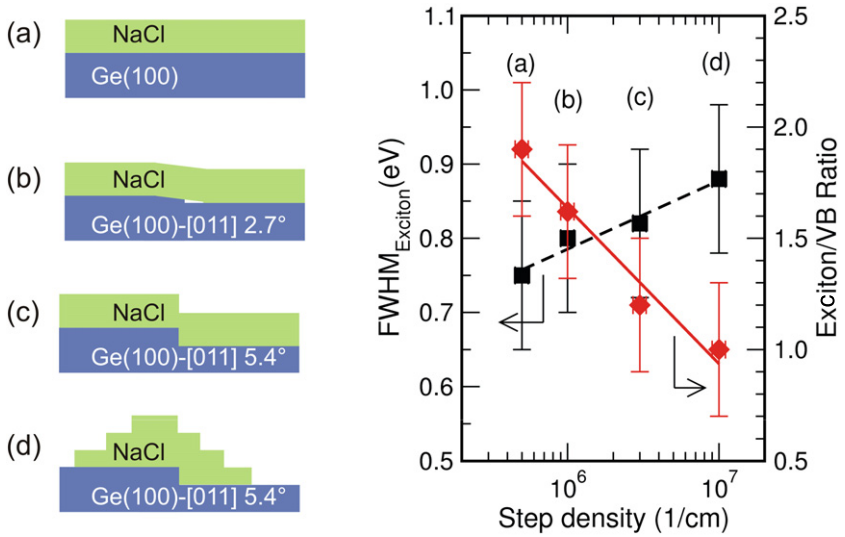

Figure 7. FWHM of the excitonic state measured with EELS on an 8 ML NaCl film (left scale) and relative peak intensity of the exciton relative to the valence band (right scale) as a function of the step density. The step densities have been derived from SPA-LEED. The different step densities were realized by different growth modes: (a) flat NaCl(100), (b) carpet structure (NaCl/Ge(100)-[011]-2.7° grown at 150 K), (c) (611) facet structure with polar steps (NaCl/Ge(100)-[011] 5.4° grown at 150 K, Si precovered), (d) pyramidal growth (NaCl/Ge(100)-[011] 5.4° grown at RT).

by EELS, only neutral and singly ionized color centers can be detected in the case of MgO.

As mentioned above, MgO films grown epitaxially on Ag(1, 1, 19) contain a significantly higher step density compared with those grown on Ag(100). The generation of four distinct losses at 2.0, 2.4, 2.8 and 3.4 eV and a broad loss centered at 5.5 eV have been observed. The latter can be attributed to bulk color centers F_B centers as deduced from their annihilation kinetics [77]. By comparing the measured loss energies with experiments performed on MgO/Ag(100) and with literature data [74, 66, 75], the observed losses at 2.0 and 2.8 eV can be consistently assigned to transitions of color centers located on step sites, whereas those at 2.4 and 3.4 eV are attributed to terrace sites (cf figure 8).

The kinetics of color center formation during electron bombardment as well as the annihilation of F-centers by simple exposure to O_2 gas at room temperature was determined and compared for differently coordinated color centers. The defect densities can be well described by $n_s \sim (1 - e^{cD})$, where D is the electron dose. Since $n_s \sim D^2$ dependences have not been found, the formation of M- or R-centers on MgO is not the dominant process during defect generation, at least at room temperature. In contrast to NaCl [78], the partial covalent character between the Mg and O atoms prevents the formation of higher aggregates. Recent electron paramagnetic resonance (EPR) and STM investigations have shown that for sufficiently high doses the ionization of neutral F_S centers is possible [75].

The influence of steps on insulating films towards any chemical reactivity has been tested by thermal desorption (TD) spectra of CO_2 molecules adsorbed on vicinal NaCl(100) films. Dissociation of, for example, H_2O molecules, as has been observed in the presence of color centers on NaCl [79], was not found for any kind of steps on these templates. Exemplarily, figures 9(b) and (c) show TD spectra of CO_2 adsorbed on a polar stepped and pyramidally stepped NaCl structure. To compare these results the TD spectra obtained from perfect NaCl(100) (figure 9(a)) and with color centers covered NaCl(100) films (figure 9(d)) are also shown. An isosteric analysis on the perfect and undamaged surface have revealed a desorption energy of $E_d = 31 \pm 2$ kJ mol^{-1} and an attempt frequency of $\log k_0 = 15.5 \pm 0.5$ Hz [80]. Furthermore, the zeroth-order desorption kinetics points towards the coexistence of a 2D gas and 2D islands on the flat and undamaged NaCl(100) surface.

To get a deeper insight into the step-induced changes of the bonding mechanism, the shifting of the desorption peak to higher temperatures and its asymmetry has been simulated. Quantitative agreement was obtained by assuming first-order desorption and a coverage-independent prefactor at low coverages. With these assumptions the desorption spectra up to 0.3 ML can be fitted with a linearly decreasing effective energy of desorption between zero coverage and 0.14 ML, starting at 34 kJ mol^{-1} at zero coverage and ending at the same value as at high coverages. On the surfaces with the pyramidal NaCl structures grown at room temperature a similar behavior has been found (figure 9(c)), but in addition a separate peak at a desorption temperature of 115 K is seen that does not exist on the flat NaCl films. This peak contains approximately 0.08 ML of CO_2, which is in the range expected for adsorption at step edges on these surfaces. With the same assumptions as just mentioned an effective desorption energy of 38 kJ mol^{-1} is deduced for this peak.

Since the step-induced modifications of the main desorption peak of CO_2 is very similar on both kinds of stepped NaCl films, and since the polar steps are expected to have an even stronger influence on the bonds of adsorbed molecules, it seems that the modifications of the main desorption peak reflect only the influence of these defects on molecules

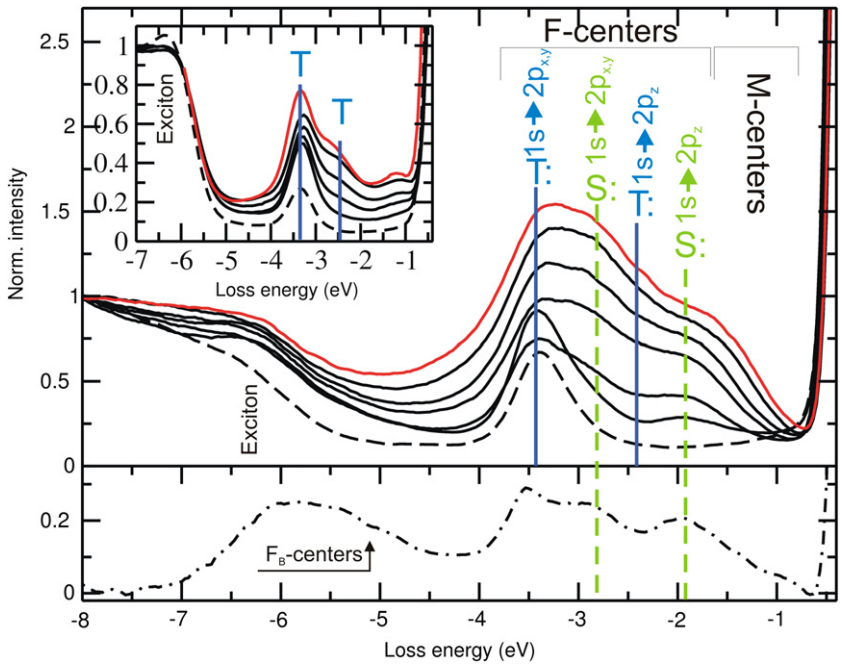

Figure 8. EEL spectra of color centers generated by electron bombardment at 150 eV incident energy as a function of increasing electron dose from bottom to top on MgO films (8 ML) grown on Ag(1, 1, 19): 70, 140, 200, 380, 830, 1280, 2180 and 3980 electrons per surface oxygen ion. The dashed curves are measured immediately after growth. The tentative assignments of transitions are marked by vertical lines for color centers located on a terrace site (T) and for those located at steps (S). The inset shows a reference spectra of F-centers generated on flat MgO(100) films. The lowest dashed–dotted curve marks the difference spectrum between the first two curves shown. The intensity most likely due to bulk (F_B) centers is marked with an arrow. The excitonic state on MgO at 6.2 eV is much less pronounced on the vicinal and irradiated surfaces than on the flat Mg(100) surface (cf the excitonic state for NaCl in figure 7).

adsorbed in their vicinity, but not directly on them. Presumably due to the high reactivity of the polar steps, the desorption spectra obtained from these surfaces are not characteristic of the desorption of CO_2 molecules directly adsorbed on these polar steps. In contrast, the desorption from the rough NaCl surfaces grown at room temperature seems to be characteristic for the non-polar steps.

3. Metallic wires on vicinal semiconductors

Despite the progress made for growing vicinal, wide bandgap surfaces, the step structure of these templates is still not perfect to grow, for instance, sufficiently long atomic wires on a mesoscopic scale. Instead a functioning approach is the use of semiconductor substrates, which are electronically insulating for appropriate dopants and concentrations, and therefore suitable for transport measurements, at least for temperatures below 200 K.

The ability to start any adsorption experiments with an almost perfect step structure of the support itself by using vicinal Si substrates was already mentioned [50, 51]. Their specific energetics and anisotropy in diffusion during growth reveal the possibility to grow one-dimensional metallic chain structures with extremely high aspect ratios, as has been demonstrated for a variety of adsorbates (Au, Ag, Gd, In, Pb, Pt, etc) on vicinal Si and Ge substrates [82–86]. Their one-dimensional character has been impressively demonstrated by photoelectron spectroscopy. In order to sustain the 1d character, typically submonolayer coverages are used. For more details the reader is referred to the overview article by Himpsel *et al* [81].

The motion of electrons within these extremely confined systems exhibit a variety of unconventional phenomena, e.g. Luttinger liquids, i.e. the bosonization of strongly interacting fermions [44], and charge density waves [45]. However, these phenomena are usually accompanied by instabilities due to enhanced electron–electron and electron–phonon interactions, e.g. at low temperatures the opening of a Peierls gap results in a metal–insulator transition as expected for many systems [48]. This correlation between the (local) structure and electronic structure has been analyzed in the past mainly by STM/STS and ARPES [87–89]. But still, there are examples where the structural nature of transition has not been clarified yet, e.g. for In/Si(111) the $(4 \times 1) \rightarrow (8 \times 2)$ transition is still discussed as a displacive or Peierls-type phase transition [87, 88, 90].

There is still a lack of transport measurements which could probe directly the above-mentioned properties of those strongly confined electrons. Only recently transport studies of nanostructures on surfaces have attracted notice to research [91, 92, 53] last but not least as the development of appropriate tools for contacting these objects have made great progress [93]. Besides the problem of making suitable ohmic contacts to these atomic wires, one still has to consider that the total surface conductivity σ is *a priori* composed of the conductivity given by the metallic film σ_{film}, the conductivity through surface states σ_{SS} (at both interfaces) and space charge

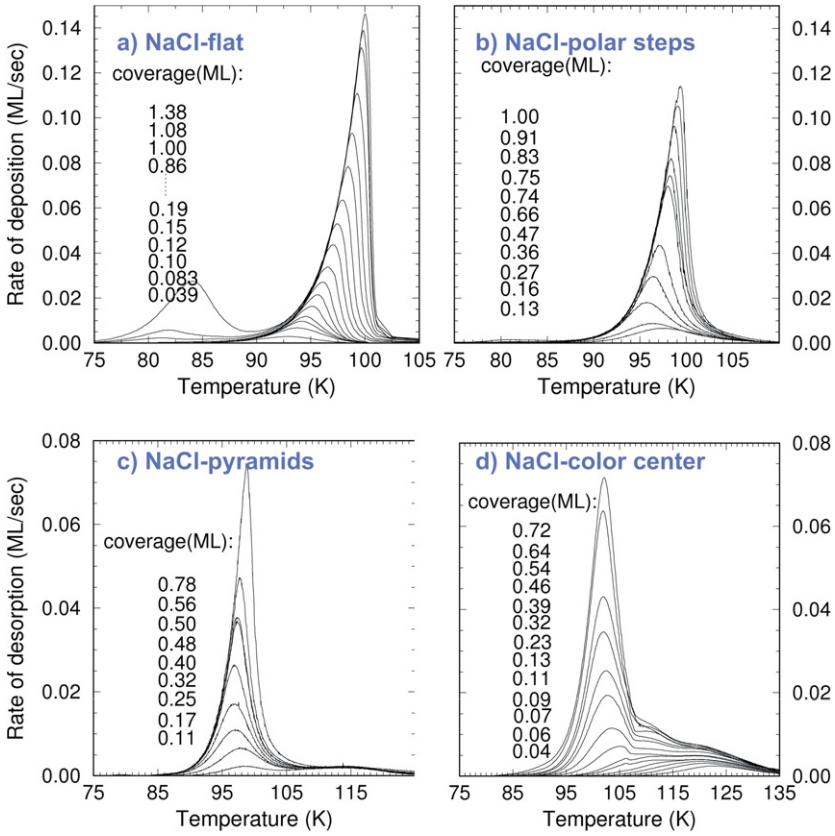

Figure 9. Desorption of CO_2 from differently stepped NaCl(100) films: (a) flat NaCl(100) as reference [80], (b) NaCl with polar steps, (c) NaCl with non-polar steps, (d) NaCl with color centers (saturation concentration around 0.1 ML). The heating rate was 0.5 K s^{-1} (1 K s^{-1} in (d)).

layers σ_{SC} [52, 53]. Considering only adsorbate layers with monolayer thicknesses, the σ_{film} and σ_{SS} contributions are equivalent. By a certain combination of an adsorbate/substrate system, space charge contributions can be avoided due to the formation of a sufficiently high Schottky barrier at the interface.

One system, which fulfills these requirements, is the monolayer structure of Pb adsorbed on Si(557). Results concerning the morphology, the corresponding electronic structure and transport properties will be summarized in the following. The structure of the different Pb phases has been controlled mainly by LEED, as this method reveals an average of the atomic structure taken on a macroscopic scale, which is important in the context of macroscopically performed transport measurements presented thereafter.

3.1. Growth of atomic chains by self-assembly

Atomic Pb chains can be generated by adsorption of 1.3 ML of Pb on a vicinal Si(557) substrate and subsequent annealing to 640 K. Already the clean substrate itself is thereby interesting from the point of its equilibrium structure, because the Si(557) is an unequally stepped surface. It consists locally of (111) and (112) facets, yielding an overall unit cell of 17 atomic units along the $[\bar{1}\bar{1}2]$ direction (5.7 nm, cf figure 10(c)). Owing to the (111) mini-terrace, low energy electron diffraction (LEED) reveals uniaxially elongated seventh-order spots, while the half-order spots stem from dimerization at the step edges of the (112) facets. A characteristic LEED pattern taken at 96 eV (scattering phase $S = 5$, step height $d = 3.14$ Å) is shown in figure 10(a). The large unit cell is seen best by the spot splitting of 5.8% SBZ of the integer spots in the $[\bar{1}\bar{1}2]$ direction. Details about further reconstructions at step edges and terrace sites of the Si(557) were recently obtained by STM measurements [94].

Adsorption of metallic adlayers on semiconducting surfaces lead in general to strong hybridization effects at the interface accompanied by strong relaxation processes. For instance, submonolayers of Au adsorbed on Si(335), Si(557), etc, surfaces exchange with the Si atoms, i.e. the Au chains are incorporated into the first atomic layer, while Si is atop [97–99]. In the case of Pb adsorption of around 1.3 ML on Si(557) the subsequent annealing to 640 K annihilates the (7×7) reconstruction of the Si(111) mini-facets and a characteristic Pb reconstruction appears. As is evident from the LEED pattern shown in figure 10(b), the most striking feature is the spot splitting with a distance between the spots of $\Delta k_y = 21.3\%$ SBZ in the $[\bar{1}\bar{1}2]$ direction at temperatures below 78 K. A detailed analysis has shown that this spot splitting corresponds to a (223) facet orientation rather than to the former (557) orientation. This is supported by recent STM measurements [100] (cf inset in figure 10(b)). As depicted schematically in figure 10(d) the steps are homogeneously distributed after the adsorption of Pb and the terraces are now

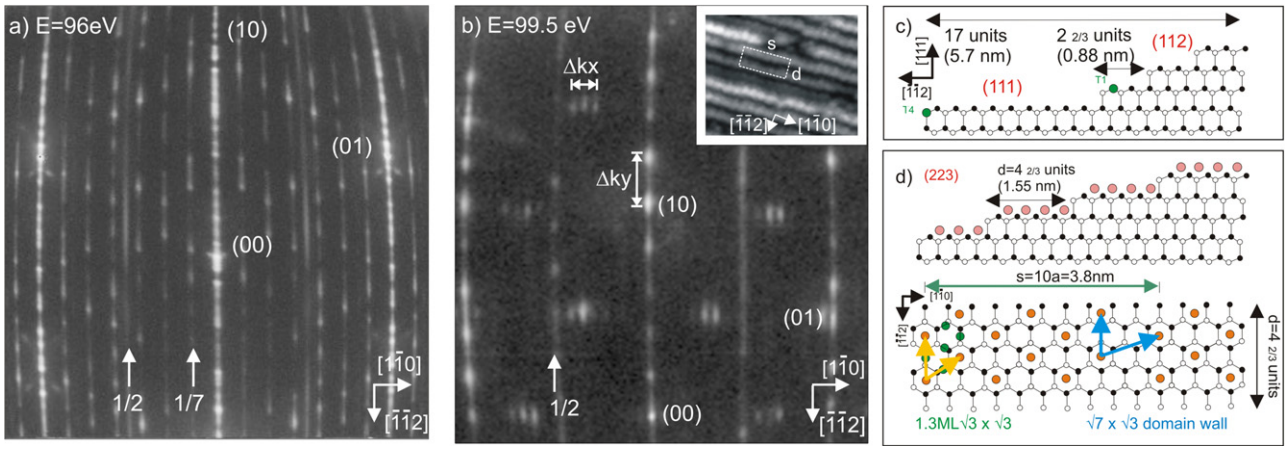

Figure 10. LEED picture of the clean Si(557) surface (a) and after adsorption and thermal annealing of 1.3 ML Pb (b). The inset shows the corresponding STM measurement of the Pb chain structure (interchain spacing 1.55 nm). The measurements were taken at 40 K. (c) and (d) show schematics of the clean surface and the surface after adsorption of 1.3 ML Pb, respectively. The light gray (orange) circles denote Pb atoms on H3 positions. The full monolayer structure is shown only for the first $\sqrt{3} \times \sqrt{3}$ unit cell. The Pb/Si(557) system provides a variety of different phases and reorientations. A detailed phase diagram can be found in [96].

$4\frac{2}{3}$ atomic units, i.e. 1.55 nm, wide. The mismatch between both orientations can be compensated by either larger (111) facets in between or by facets with the opposite inclination angle.

Beyond that, the Pb/Si(557) system shows a strong coverage dependence. By varying the Pb concentration on the surface, the interchain distance and the modulation periodicity can be tuned gradually as a function of coverage between 1.2–1.6 ML. Interestingly, the (557) orientation itself is metastable in the presence of Pb. A detailed phase diagram of the Pb/Si(557) system can be found in [96]. Nonetheless, among these different Pb phases on Si(557), only the (223) facet structure reveals a nearly equally distributed step structure and only this turns out to be energetically favored, supported by angle-resolved photoemission results [102, 95].

As is also obvious from figure 10(b), superstructure spots at $\sqrt{3} \times \sqrt{3}$ positions appear, which are split by $k_x \approx 10\%$ SBZ in the [1$\bar{1}$0] direction. A schematic of this phase is shown in the lower part of figure 10(d). This periodicity along the chain is caused by regularly arranged domain walls. On each terrace, this so-called (1, 5) linear phase consists of 5 $\sqrt{3} \times \sqrt{3}$, separated by one $\sqrt{7} \times \sqrt{3}$ domain wall. The steps are assumed to be not decorated by Pb atoms, which is important in the context of the temperature-driven refaceting process (see below). The linear phases, also known as the devil's staircase, have been found first on nominally flat Si(111) surfaces for all three domains [101]. We will see in the next section that this rearrangement on a mesoscopic scale by Pb adsorption in both directions is essential for the transport properties found for this system.

3.2. Transport properties

To emphasize the above-mentioned correlation between structure and functionalization, we performed macroscopic conductivity experiments in an extended van der Pauw geometry on these samples. Eight macroscopic $TiSi_2$ contacts with a thickness of approximately 50 nm were deposited onto the Si(557) sample prior to insertion into the UHV chamber. The separation between equivalent contacts was approximately 10 mm. A schematic is shown in figure 11. The use of eight contacts allow exact symmetrization of the current parallel and normal to the step direction. By a software-controlled switching between equivalent sets of contacts, the conductivity was measured sequentially parallel and perpendicular to the steps. In all measurements contributions of the clean Si substrate were carefully subtracted (of the order of μS below 180 K). Although the realizations of these contacts is difficult, they act as ideal point contacts due to their arrangement and the problem of injecting hot electrons is avoided, too.

A typical conductance measurement of the Pb wire phase on Si(557) is shown in figure 11. A systematic transport study by varying the initial Pb coverage has shown [103] that at least one physical monolayer, i.e. 1.3 ML with respect to the Si(111) substrate, is necessary to observe (i) an anisotropic 2d regime above T_c, where activated transport is found in both directions, (ii) a reversible transition in conductivity occurring at $T_c = 78$ K and (iii) a 1d regime, where only along the wires is a metallic, i.e. $1/T$ temperature dependence, found. Moreover, this quasi-1D metallic conductance state at low temperature exhibits no indications of further instabilities, at least down to 4 K. Compared to many other systems, where the atomic chain structure is seen also by spectroscopy, i.e. dispersion of electrons is seen only along the wire structure [81, 82, 84], the Pb/Si(557) is spectroscopically truly two-dimensional, as revealed by angle-resolved photoelectron spectroscopy [95, 102]. This points towards a strong coupling of the Pb wires and avoids presumably the expected instabilities within purely 1d systems.

The one-dimensional conductance found for this layer at low temperatures below 78 K is thus caused by this particular (223) facet structure. As obtained from ARPES measurements, the perfect arrangement of these steps on a mesoscopic scale give rise electronically to perfect Fermi nesting in the direction

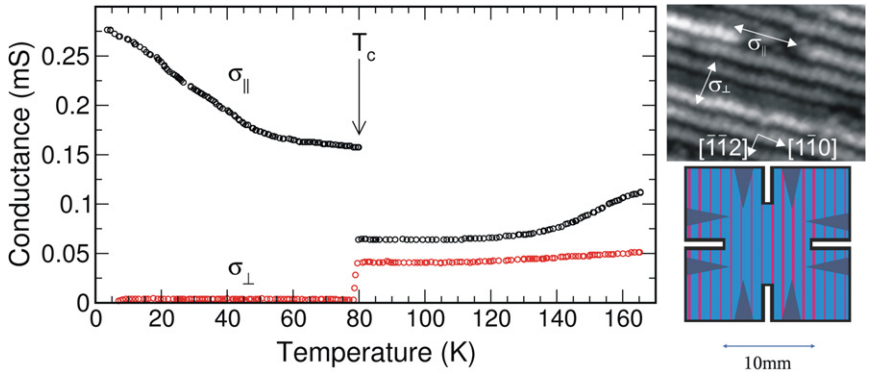

Figure 11. Conductance curve obtained for 1.3 ML Pb on Si(557) after subsequent annealing to 640 K. The modified eight-point contact geometry as depicted on the lower right allows us to measure independently the conductance along ($\sigma_\parallel$) and across ($\sigma_\perp$) the wires (cf STM picture on the upper right).

across the wires rather than by localization due to confinement of the electrons in single wires. The ARPES study has shown further that along the wires split-off bands cause the 1d conductance [102]. The intersections of these branches at Fermi energy coincide almost with the Γ points of the mesoscopic periodicity defining the tenfold periodicity of the (1, 5) linear phase along the $[1\bar{1}0]$ direction. Thus the insensitivity of the dc conductance to atomic defects in the Pb chains found in experiment [103] can be explained by the extremely long Fermi wavelength ($\lambda_F \geqslant 20$ nm) of this conduction band. As mentioned, below T_c the (223) facet structure is electronically stabilized as seen by the nested points of the Fermi surface. The accompanying gap could be estimated to be around 20 meV, which is of the expected order of magnitude for a transition temperature of 78 K seen for the conductance measurements.

3.3. Switching of the conductance by a phase transition

The abrupt switching in conductance to a weakly anisotropic two-dimensional system at higher temperature is due to a temperature-driven structural change [104]. The relevant results are summarized in figure 12 for the $[\bar{1}\bar{1}2]$ direction, i.e. across the wire direction, where the insulator–semiconductor transition appears in transport (cf red (lower) curve in figure 11). As revealed from STM measurements and LEED (cf figure 10(b)) this structure belongs at low temperatures to a (223) facet. The temperature-induced change of the spot splitting can be seen best by line scans taken along the $[\bar{1}\bar{1}2]$ direction (cf figure 12(a)). Note that the Pb-induced (223) facet structure of the initial (557) oriented surface can be either compensated by facets of the opposite inclination or by larger (111) facets, which were generated here accidentally during the high annealing steps of the sample preparation. However, the (10) spot of these (111) facets can be conveniently used to determine exactly the facet orientation by plotting the spot positions as a function of scattering phase. Figure 12(b) shows such a ($k_\perp$, $k_\parallel$) plot taken around the (662) Bragg point. For the measurement at 4 K the angle in between the rods is $\theta = \arctan(k_\parallel/k_\perp) = 11.4° \pm 0.3°$, in almost perfect agreement with a (223) facet. At 80 K, this angle changes to $10.5° \pm 0.3°$, which is within error bars compatible with a (17 17 25) orientation. This proves the temperature-dependent reorientation of the whole surface and excludes demixing of different facet orientations on the surface. More details about this temperature-induced refaceting orientation can be found in [104].

The abrupt switching in conductance to a weakly anisotropic two-dimensional system at a higher temperature is due to a breakdown of the perfect nesting condition, which has its origin in these structural changes upon annealing. The destruction of the perfect Fermi nesting is confirmed by ARPES, showing a loss of intensity at E_F at the nesting points defined by the modulated Pb wire structure. The LEED experiments reveal that the terrace structure is only slightly modified above the phase transition, since the average terrace width is only changed by 4%, and it remains stable above the transition temperature. This result about the local terrace structure is corroborated by STM measurements [105]. The average change in lattice constant, however, is almost impossible to visualize with STM[1].

The appearance of the transition itself depends crucially on the coverage. In figure 13 is plotted the spot splitting Δk_y versus the temperature measured for three different Pb coverages. The refaceting transition occurs only at 1.3 ML, i.e. where only the terraces but not the steps are decorated. For lower coverages around 1.24 ML, instead of the (223) a (335) facet has been found by LEED, i.e. the above-mentioned Fermi nesting cannot take place to stabilize this phase at all. We have recently shown that, by adsorption of an additional 0.1 ML onto the 1.3 ML Pb, every second step (step concentration is 20%) is decorated with additional Pb as judged from the doubling of the periodicity given by the (223) facet structure. As adsorption goes on, the doubling vanishes and the former (223) facet structure almost reappears in LEED [96]. According to figure 13, this refaceting transition

[1] To go from a (223) to a (17 17 25) facet structure means to add one row of atoms every six terraces on average in a fluctuating system. Therefore, averages over several hundred terraces are necessary to safely detect such a small change, which in addition is not static on STM timescales. This means that STM is most likely too slow for detection of a snapshot, but also does not take a reasonable average. This is the reason why we have called this refaceting transition an order–disorder transition in former publications [105].

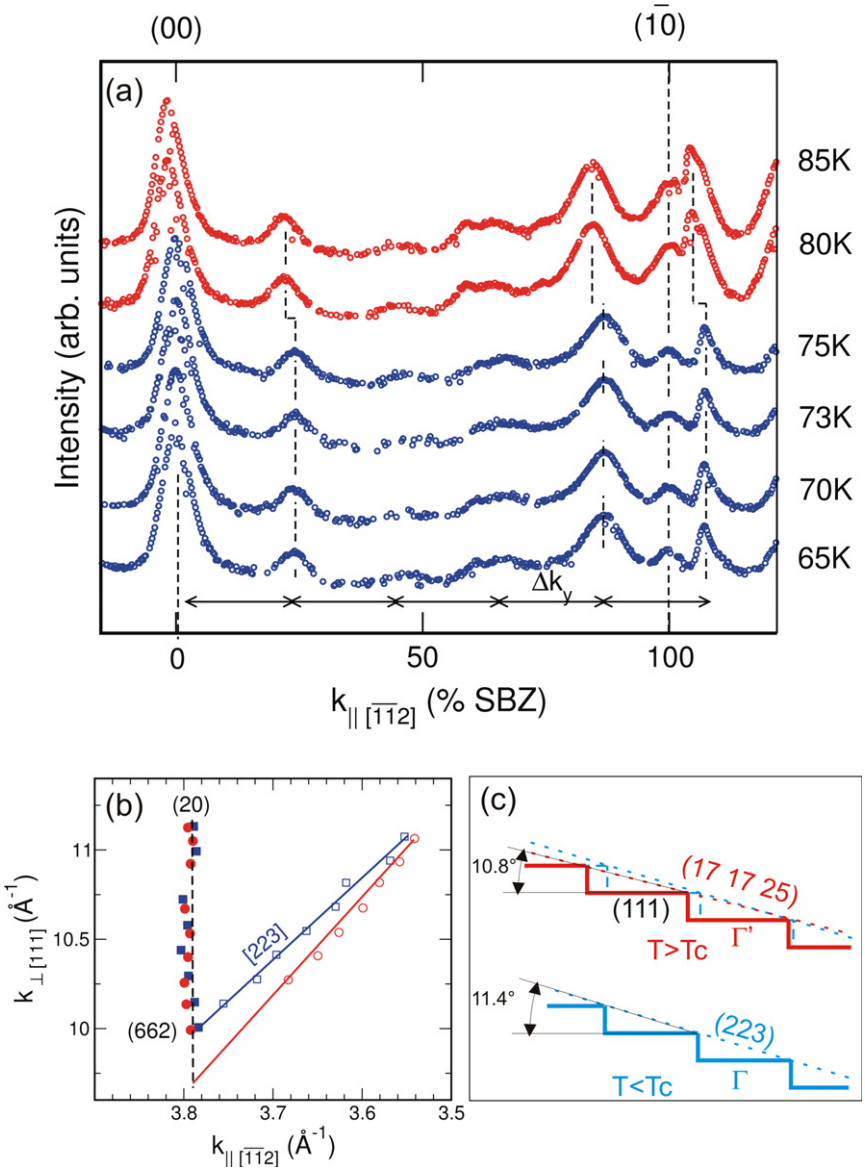

Figure 12. (a) Line scans along the $[\bar{1}\bar{1}2]$ direction (see figure 10) taken below and above the transition temperature ($E = 96$ eV). The temperature-driven changes in the spots are due to a refaceting process. (b) ($k_\perp$, $k_\parallel$) plot around the (662) Bragg point, showing the transition from a (223) facet structure to a (17 17 25) facet structure. The change of the inclination angle is depicted schematically in (c).

is completely suppressed when at least all steps are decorated. In the case of a partial decoration, e.g. 1.45 ML, the transition is seen only weakly (see inset in figure 13). In the case that all steps are decorated, the 'ideal' (223) facet structure is slightly changed towards an larger average terrace length. This small coverage-driven change is in line with strong refacetings found ((112) → (335) → (223)) while changing the Pb coverage from 1.2 to 1.6 ML [96].

The Pb/Si(557) system is a fascinating example of how vicinal surfaces can be functionalized. Although the nature of the 1d transport channel is still unknown, at least the origin of the 1d conductance within these coupled 2d system, i.e. wires, and the switching in conductance by a refaceting transition could be clarified. However, these intriguing structural and transport properties occur only when 'shortcuts' between the wires are suppressed.

4. Summary and future perspectives

In summary, towards the functionalization of vicinal surfaces, the focus of this review was basically towards the growth of vicinal insulating films on conducting substrates and the growth of metallic chains on low-doped semiconductor substrates. The growth of wide bandgap insulating and vicinal films has been demonstrated for CaF_2, NaCl, MgO and mixed $Ba_{0.3}Sr_{0.7}O$ films. The critical parameters are the vertical and lateral lattice accommodation. The specific properties of these stepped structures have been proven by studying their defect kinetics and impact towards adsorption.

The step structure of vicinal Si(111) substrates can be controlled much better and growth of metallic wires with extremely high aspect ratios is possible. As demonstrated for Pb/Si(557) even transport measurements on a macroscopic

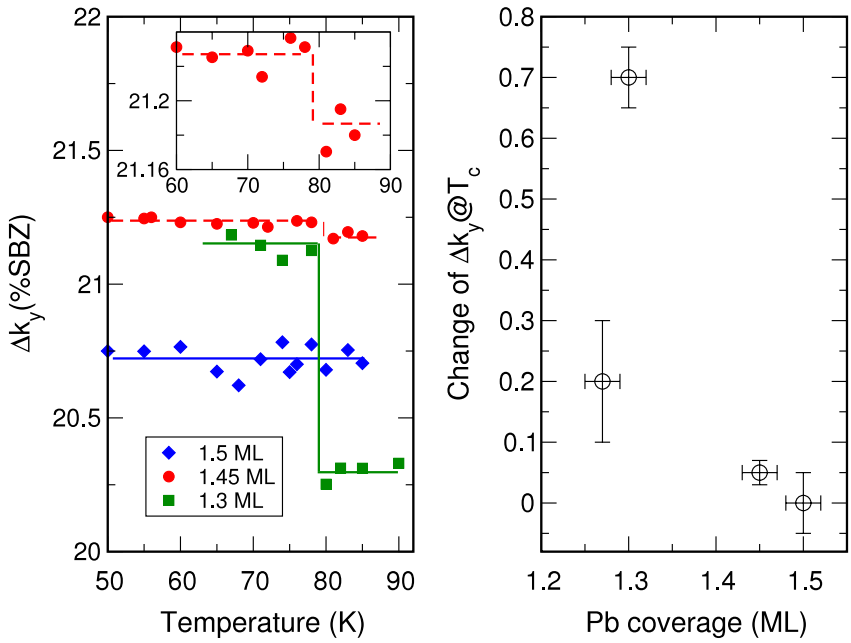

Figure 13. Average spot splitting Δk_y (cf figure 10) as a function of temperature for different Pb coverages. The refaceting transition is seen best for the 1.3 ML coverage, i.e. where the steps are not decorated.

scale can be performed. The system shows nicely the important interplay between morphology and electronic structure and how this determines the transport properties. However, these properties depend crucially on the interaction between the wires, which are, on the other hand, obviously of importance to avoid instabilities in these low-dimensional chain structures.

As a result of the lattice mismatch and defects of the underlying substrates, the vicinal insulating films are still too imperfect to grow ultra-long atomic wires suitable for transport. This is still challenging and most promising so far are the mixed BaSrO films and the CaF_2 films, as they can be grown almost perfectly lattice-matched on defect-free Si(100) and Si(111) substrates. Nonetheless, the stepped films presented above can be used to study the adsorption of metallic clusters and molecules in the presence of short but well-defined step structures (polar and non-polar) and test, for instance, their enhanced chemical activity. The insulating films are obtained already for a thickness of a few monolayers and are therefore accessible to STM/STS, giving rise to manipulation of molecules and other nano-objects and probing their electronic structure, as has been demonstrated recently on flat insulating films [40].

Alternatively, to use directly the surfaces of bulk insulating materials has not been considered in this review further, also because many surface science techniques are not applicable. Despite the technical problem of making arbitrarily stepped surfaces by an *in situ* cleavage, the step structures themselves are quite perfect and single steps can be decorated with metallic chain structures. The atomic force microscopy with its capability of atomic resolution on insulators [106, 107] may attract more notice to this research in future and may be used also for manipulation of nanosized clusters on an atomic scale.

Acknowledgments

I want to take the opportunity to thank my supervisor Herbert Pfnür for stimulating discussions and his outstanding support and all my colleagues who contributed to these measurements and results, in particular: Ziad Kallassy, Judith Kramer, Winfried Ernst, Marcin Czubanowski, Annemarie Schuster, Jan Zachariae, Tammo Block and Joachim Wollschläger. Further I would like to acknowledge the Deutsche Forschungsgemeinschaft, the Volkswagen Foundation and the K+S Company for their financial support over the last few years.

References

[1] http://apps.isiknowledge.com
[2] Avouris P and Wolkow R 1988 *IBM Research Report* No. RC 13884
[3] Bauer E, Telieps W and Turner G 1988 *J. Vac. Sci. Technol.* A **6** 573
[4] Latyshev A V, Aseev A L, Krasilnikov A B and Stenin S I 1990 *Surf. Sci.* **227** 24
[5] Suzuki T, Metois J J and Yagi K 1995 *Surf. Sci.* **339** 105
[6] Tegenkamp C, Wollschläger J, Pfnür H, Meyer zu Heringdorf F J and Horn-von Hoegen M 2002 *Phys. Rev.* B **65** 235316
[7] Wollschläger J and Tegenkamp C 2007 *Phys. Rev.* B **75** 245439
[8] Jörgenson L and Harris R 1993 *Phys. Rev.* E **47** 3504
[9] Bartelt N C, Einstein T L and Williams E D 1994 *Surf. Sci.* **312** 411
[10] Wilson K G 1975 *Rev. Mod. Phys.* **47** 773
[11] Gruber E E and Mullins W W 1967 *J. Phys. Chem. Solids* **28** 875
[12] Kan H C, Kwon T and Phaneuf R J 2008 *Phys. Rev.* B **77** 205401
[13] Jeong H C and Williams E D 1999 *Surf. Sci. Rep.* **34** 171
[14] Gartland P O and Slagsvold B J 1975 *Phys. Rev.* B **12** 4047

[15] Tersoff J and Kevan S D 1983 *Phys. Rev.* B **28** 4267
[16] McDougall B A, Balasubramanian T and Jensen E 1995 *Phys. Rev.* B **51** 13891
[17] Matzdorf R, Meister G and Goldmann A 1996 *Phys. Rev.* B **54** 14807
[18] Mugarza A, Ortega J E, Himpsel F J and Garcia de Abajo F J 2003 *Phys. Rev.* B **67** 081404
[19] Didiot C, Fagot-Revurat Y, Pons S, Kierren B, Chatelain C and Malterre D 2006 *Phys. Rev.* B **74** 081404(R)
[20] Rousset S, Repain V, Baudot G, Garreau Y and Lecoeur J 2003 *J. Phys.: Condens. Matter* **15** S3363
[21] Roth M, Fauster T and Weinelt M 2007 *Appl. Phys.* A **88** 497
[22] Mugarza A and Ortega J E 2003 *J. Phys.: Condens. Matter* **15** S3281
[23] Kuhnke K and Kern K 2003 *J. Phys.: Condens. Matter* **15** S3311
[24] Pratzer M, Elmers H J, Bode M, Pietzsch O, Kubetzka A and Wiesendanger R 2001 *Phys. Rev. Lett.* **87** 127201
[25] Gambardella P, Dallmeyer A, Maiti K, Malagoli M C, Rusponi S, Ohresser P, Eberhardt W, Carbone C and Kern K 2004 *Phys. Rev. Lett.* **93** 077203
[26] Gambardella P, Dallmeyer A, Maiti K, Malagoli M C, Eberhardt W, Kern K and Carbone C 2002 *Nature* **416** 301
[27] Shiraki S, Fujisawa H, Nantoh M and Kawai M 2005 *Phys. Rev. Lett.* **92** 096102
Shiraki S, Fujisawa H, Nantoh M and Kawai M 2005 *J. Phys. Soc. Japan* **74** 2033
[28] Negulyaev N N, Stepanyuk V S, Hergert W, Bruno P and Kirschner J 2008 *Phys. Rev.* B **77** 085430
[29] Cheng R, Bader S D and Fradin F Y 2008 *J. Appl. Phys.* **103** 07B729
[30] Hahlin A, Dunn J H, Karis O, Poulopoulos P, Nünthel R, Lindner J and Arvanitis D 2003 *J. Phys.: Condens. Matter* **15** S573
[31] Langmuir I 1918 *J. Am. Chem. Soc.* **40** 1361
[32] Taylor H S 1925 *Proc. R. Soc. Lond.* A **108** 105
[33] Smoluchkowski R 1941 *Phys. Rev.* **60** 661
[34] Tersoff J and Falicov L M 1981 *Phys. Rev.* B **24** 754
[35] Hammer B and Nørskov J K 2000 *Adv. Catal.* **45** 71
[36] Yates J T Jr 1995 *J. Vac. Sci. Technol.* A **13** 1359
[37] Zambelli T, Trost J, Wintterlin J and Ertl G 1996 *Phys. Rev. Lett.* **76** 795
[38] Gambardella P, Šljivančanin Ž, Hammer B, Blanc M, Kuhnke K and Kern K 2001 *Phys. Rev. Lett.* **87** 056103
[39] Tegenkamp C and Pfnür H 2002 *Phys. Chem. Chem. Phys.* **4** 2653
[40] Repp J, Meyer G, Olsson F E and Persson M 2004 *Science* **305** 493
[41] Abbet S, Sanchez A, Heiz U, Schneider W-D, Ferrari A M, Pacchioni G and Rösch N 2000 *J. Am. Chem. Soc.* **122** 3453
[42] Pacchioni G, Giordano L and Baistrocchi M 2005 *Phys. Rev. Lett.* **94** 226104
[43] Korin-Hamzic B, Tafra E, Basletic M, Hamzic A and Dressel M 2006 *Phys. Rev.* B **73** 115102
[44] Luttinger J M 1963 *J. Math. Phys.* **4** 1154
[45] Carpinelli J M, Weitering H H, Plummer E W and Stumpf R 1996 *Nature* **381** 398
[46] Mermin N D and Wagner H 1966 *Phys. Rev. Lett.* **17** 1133
[47] Block T and Pfnür H 2008 *J. Appl. Phys.* **103** 064393
[48] Pfnür H 2008 *Surf. Sci.* **602** 1727
[49] Gardinowski G, Schmeidel J, Pfnür H, Block H and Tegenkamp C 2006 *Appl. Phys. Lett.* **89** 063120
[50] Viernow J, Lin J L, Petrovykh D Y, Leibsle F M, Men F K and Himpsel F J 1998 *Appl. Phys. Lett.* **72** 9498
[51] Kirakosian A, Bennewitz R, Crain J N, Fauster T, Lin J L, Petrovykh D Y and Himpsel F J 2001 *Appl. Phys. Lett.* **79** 1608
[52] Hirahara T, Matsuda I, Yamazaki S, Miyata N, Nagao N and Hasegawa S 2007 *Appl. Phys. Lett.* **91** 202106
[53] Matsuda I and Hasegawa S 2007 *J. Phys.: Condens. Matter* **19** 355007
[54] Schwoebel R L and Shipsey E J 1966 *J. Appl. Phys.* **37** 3682
[55] Ehrlich G and Hudda F G 1966 *J. Chem. Phys.* **44** 1039
[56] Wollschläger J 2002 *Appl. Phys.* A **75** 155
[57] Viernow J *et al* 1999 *Appl. Phys. Lett.* **74** 2125
[58] Hessinger U, Leskovar M and Olmstead M A 1995 *Phys. Rev. Lett.* **75** 2380
[59] Denlinger J D, Rotenberg E, Hessinger U, Leskovar M and Olmstead M A 1995 *Phys. Rev.* B **51** 5352
[60] Klust A, Bierkandt M, Wollschläger J, Müller B H, Schmidt T and Falta J 2002 *Phys. Rev.* B **65** 193404
[61] Kramer J, Tegenkamp C and Pfnür H 2003 *Surf. Sci.* **537** 265
[62] Tegenkamp C, Ernst W, Eichmann M and Pfnür H 2000 *Surf. Sci.* **466** 41
[63] Zachariae J and Pfnür H 2006 *Surf. Sci.* **600** 2785
[64] Wollschläger J, Erdös D, Goldbach H, Höpken R and Schröder K M 2001 *Thin Solid Films* **400** 1
[65] Wollschläger J, Viernow J, Tegenkamp C, Erdös D, Schröder K M and Pfnür H 1999 *Appl. Surf. Sci.* **142** 129
[66] Kramer J, Ernst W, Tegenkamp C and Pfnür H 2002 *Surf. Sci.* **517** 87
[67] Riemann A, Fölsch S and Rieder K H 2005 *Phys. Rev.* B **72** 125423
[68] Fölsch S, Riemann A, Repp J, Meyer G and Rieder K H 2002 *Phys. Rev.* B **66** 161409
[69] Schwennicke C, Schimmelpfennig J and Pfnür H 1993 *Surf. Sci.* **293** 57
[70] Glöckler K, Sokolowski M, Soukopp A and Umbach E 1996 *Phys. Rev.* B **54** 7705
[71] Tegenkamp C and Pfnür H 2003 *Surf. Sci.* **574** 205
[72] Zachariae J and Pfnür H 2005 *Phys. Rev.* B **72** 075410
[73] Al-Falou A A, Kammler M and Horn von Hoegen M 2005 *Europhys. Lett.* **69** 570
[74] Sousa C, Pacchioni G and Illas F 1999 *Surf. Sci.* **429** 217
[75] Sterrer M, Fischbach E, Heyde M, Nilius N, Rust H P, Risse T and Freund H J 2006 *J. Phys. Chem.* B **110** 8665
[76] Avigin I and Huber D L 2008 *J. Lumn.* **128** 1623 (see also arXiv:cond-mat/0512339v1)
[77] Kramer J, Tegenkamp C and Pfnür H 2003 *Phys. Rev.* B **67** 235401
[78] Zielasek V, Hildebrandt T and Henzler M 2000 *Phys. Rev.* B **62** 2912
[79] Malaske U, Tegenkamp C, Pfnür H and Henzler M 1999 *Surf. Sci.* **408** 237
[80] Ernst W, Eichmann M, Budde K and Pfnür H 2000 *Surf. Sci.* **464** 35
[81] Himpsel F J, Altmann K N, Bennewitz R, Crain J N, Kirakosian A, Lin J L and McChesney J L 2001 *J. Phys.: Condens. Matter* **13** 11097
[82] Ahn J R, Yeom H W, Yoon H S and Lyo I W 2003 *Phys. Rev. Lett.* **91** 196403
[83] Crain J N, Kirakosian A, Altmann K N, Bromberger C, Erwin S C, McChesney J L, Lin J L and Himpsel F J 2003 *Phys. Rev. Lett.* **90** 176805
[84] Crain J N and Himpsel F J 2006 *Appl. Phys.* A **82** 431
[85] Schwingenschlögl U and Schuster C 2007 *Europhys. Lett.* **81** 26001
[86] Gurlu O, Adam O A O, Zandvliet H J W and Poelsema B 2003 *Appl. Phys. Lett.* **83** 4610
[87] Yeom H W, Takeda S, Rotenberg E, Matsuda I, Horikoshi K, Schäfer J, Lee C M, Kevan S D, Ohta T, Nagao T and Hasegawa S 1999 *Phys. Rev. Lett.* **82** 4898
[88] Ahn J R, Byun J H, Koh H, Rotenberg E, Kevan S D and Yeom H W 2004 *Phys. Rev. Lett.* **93** 106401

[89] Van Houselt A, Gnielka T, Aan de Brugh J M J, Oncel N, Kockmann D, Heid R, Bohnen K P, Poelsema B and Zandvliet H J W 2008 *Surf. Sci.* **602** 1731
Pfnür H 2008 *Surf. Sci.* **602** 1727 (perspective)
[90] Fleischer K, Chandola S, Esser N, Richter W and McGilp J F 2007 *Phys. Rev.* B **76** 205406
[91] Okino H, Matsuda I, Yamazaki S, Hobara S and Hasegawa S 2007 *Phys. Rev.* B **76** 035424
[92] Matsuda I, Liu C, Hirahara T, Ueno M, Tanikawa T, Kanagawa T, Hobara R, Yamazaki S, Hasegawa S and Kobayashi K 2007 *Phys. Rev. Lett.* **99** 146805
[93] Kim T W, Wang Z, Weitering H H, Wenzhi L and Li A P 2007 *Rev. Sci. Instrum.* **78** 123701
[94] Teys S A, Romanyuk K N, Zhachuk R A and Olshanetsky B Z 2006 *Surf. Sci.* **600** 4878
[95] Kim K S, Morikawa H, Choi W H and Yeom H W 2007 *Phys. Rev. Lett.* **99** 196804
[96] Czubanowski M, Schuster A, Akbari S, Pfnür H and Tegenkamp C 2007 *New J. Phys.* **9** 338
[97] Ren C Y, Tsay S F and Chuang F C 2007 *Phys. Rev.* B **76** 075414
[98] Erwin S C 2003 *Phys. Rev. Lett.* **91** 206101
[99] Crain J N, McChesney J L, Zheng F, Gallagher M C, Snijders P C, Bissen M, Gundelach C, Erwin S C and Himpsel F J 2004 *Phys. Rev.* B **69** 125401
[100] Morikawa H, Kim K S, Jung D Y and Yeom H W 2007 *Phys. Rev.* B **76** 165406
[101] Yakes M, Yeh V, Hupalo M and Tringides M C 2004 *Phys. Rev.* B **69** 224103
[102] Tegenkamp C, Ohta T, McChesney J L, Dil H, Rotenberg E, Pfnür H and Horn K 2008 *Phys. Rev. Lett.* **100** 076802
[103] Tegenkamp C, Kallassy Z, Günter H L, Zielasek V and Pfnür H 2005 *Eur. Phys. J.* B **43** 557
[104] Czubanowski M, Schuster A, Pfnür H and Tegenkamp C 2008 *Phys. Rev.* B **77** 174108
[105] Tegenkamp C, Kallassy Z, Pfnür H, Günter H L, Zielasek V and Henzler M 2005 *Phys. Rev. Lett.* **95** 176804
[106] Filleter T, Paul W and Bennewitz R 2008 *Phys. Rev.* B **77** 035430
[107] Pakarinen O H, Barth C, Foster A S, Nieminen R M and Henry C R 2006 *Phys. Rev.* B **73** 235428